3D multi-cell-type liver organoids: A new model of non-alcoholic fatty liver disease for drug safety assessments

J. Bronsard, C. Savary, J. Massart, R. Viel, L. Moutaux, Daniel D. Catheline, V. Rioux, B. Clement, A. Corlu, B. Fromenty, et al.

Toxicology in Vitro 94 (2024) 105728

Contents lists available at ScienceDirect

Toxicology in Vitro

journal homepage: www.elsevier.com/locate/toxinvit

3D multi-cell-type liver organoids: A new model of non-alcoholic fatty liver disease for drug safety assessments

J. Bronsard [a], C. Savary [b], J. Massart [a], R. Viel [c], L. Moutaux [a], D. Catheline [a], V. Rioux [a], B. Clement [a], A. Corlu [a], B. Fromenty [a], P.J. Ferron [a,*]

[a] INSERM, Université de Rennes, INRAE, Institut NuMeCan UMR1317 (Nutrition, Metabolisms and Cancer), F-35000 Rennes, France
[b] Univ Angers, CHU Angers, Inserm, CNRS, MINT, SFR ICAT, F-49000 Angers, France
[c] Univ Rennes, CNRS, Inserm, Biosit UAR 3480 US_S 018, France-BioImaging (ANR-10-INBS-04), plateforme H2P2, F-35000 Rennes, France

ARTICLE INFO

Editor name: Dr. I Maschmeyer

Keywords:
Liver organoids
NAFLD
MASLD
DILI

ABSTRACT

The development of *in vitro* models that recapitulate critical liver functions is essential for accurate assessments of drug toxicity. Although liver organoids can be used for drug discovery and toxicology, they are limited by (i) the lack of expression and activity of xenobiotic-metabolizing enzymes, and (ii) the difficulty of mimicking non-alcoholic fatty liver disease (NAFLD, which influences the expression of these enzymes) *in vitro*. Here, we generated three-dimensional multi-cell-type liver organoids (hereafter "HML organoids") from HepaRG cells, primary human macrophages, and hepatic-stellate-cell-derived LX-2 cells. We also developed an NAFLD model by culturing HML organoids for 9 days with a mixture of stearic and oleic acids. The exposed organoids showed typical features of steatosis and expressed fibrosis markers. We subsequently used HML and NAFLD-HML organoids to model drug-induced liver injury. By estimating the IC50 and benchmark doses, we were able to improve the *in vitro* detection of drugs likely to be toxic in fatty livers. Thus, HML and NAFLD-HML organoids exhibited most of the liver's functions and are relevant *in vitro* models of drug metabolism, drug toxicity, and adverse drug event in NAFLD.

1. Introduction

The administration of drugs sometimes leads to the occurrence of serious adverse events, which are associated with significant morbidity and mortality - particularly in a context of acute or chronic disease. The liver is a key organ in drug metabolism, and drug-induced liver injury (DILI) is a clinical reality (Massart et al., 2017). Importantly, various chronic liver diseases (including non-fatty alcoholic liver disease (NAFLD, recently renamed as metabolic dysfunction-associated steatotic liver disease (MASLD) (Rinella et al., 2023))) are risk factors for DILI (Fromenty, 2013). Given the increasing prevalences of obesity and NAFLD worldwide (Perumpail et al., 2017), the development of serious adverse events (such as DILI) linked to routinely prescribed drugs is becoming a major public health concern.

Primary human hepatocytes (pHHs) have been put forward as the "gold standard" model for predicting DILIs *in vitro*. Interestingly, pHHs exposed to free fatty acids (FAs) accumulate lipids and can be used as a model of steatosis (Müller and Sturla, 2019). However, pHHs have some critical limitations, such as limited availability, the progressive loss of hepatic functions, and therefore incompatibility with chronic drug exposure (Bell et al., 2017; Ruoß et al., 2020). *In vitro* models of steatosis have been developed to study the mechanisms of drug toxicity that occur in patients diagnosed with a fatty liver (Boeckmans et al., 2020; Bucher et al., 2017). The HepaRG cell line metabolizes drugs in much the same way as pHHs (Aninat, 2005), accumulates triglycerides (TGs), and exhibits metabolic changes similar to those seen in patients with non-alcoholic steatohepatitis (Le Guillou et al., 2018). Following chronic exposure to bisphenol A or rifampicin, HepaRG cells showed dose-dependent lipid accumulation and upregulation of apolipoprotein B (Allard et al., 2021; Bucher et al., 2017).

In addition to lipid accumulation, the main features of DILI are hepatocyte injury, cholestasis, steatosis, phenotypic changes in hepatic

Abbreviations: BMD, Benchmark dose; C_{max}, maximum serum concentration; DILI, Drug-induced liver injury; ECM, Extracellular matrix; FA, Fatty acid; HML, HepaRG/macrophage/LX-2; HSC, Hepatic stellate cell; IC50, Half-maximal inhibitory concentration; MASLD, Metabolic dysfunction-associated steatotic liver disease; NAFLD, Non-alcoholic fatty liver disease; pHH, Primary human hepatocyte.

* Corresponding author.
E-mail address: ferron.pj@gmail.com (P.J. Ferron).

https://doi.org/10.1016/j.tiv.2023.105728
Received 10 March 2023; Received in revised form 23 October 2023; Accepted 3 November 2023
Available online 10 November 2023

stellate cells (HSCs), and Kupffer cell activation (Khadka et al., 2020). The co-culture of HepaRG cells with the HSC-derived LX-2 cell line resulted in an accumulation of extracellular matrix (ECM), which mirrors the progression of steatosis to steatohepatitis (Dornas et al., 2019). Advances in three-dimensional (3D) tissue engineering have provided organoid models as clinically relevant tools for (i) gaining a better understanding liver functions and (ii) studying the role of non-parenchymal and parenchymal liver cells in the development of NAFLD (van Os et al., 2022) and DILI (Yan et al., 2021). When cultured on 3D substrates, HepaRG cells and HSCs form liver organoids that are suitable for the assessment of fibrogenesis (Leite et al., 2016). In 3D scaffold-free cultures or when embedded in ECM, HepaRG cells have a pHH-like metabolic phenotype, produce ECM, and have immune activity (Messner et al., 2019; Rose et al., 2021). Hence, 3D HepaRG models have been used to evaluate drug toxicity, genotoxicity (Barranger and Hégarat, 2022), steatosis induction (Teng et al., 2021), and fibrosis induction (Zahmatkesh et al., 2022), hepatocyte injury, inflammation, and fibrosis – many of which are involved in DILI. However, a 3D model for the assessment of drug toxicity in the context of NAFLD has not previously been described.

Here, we present a 3D liver organoid model that combines HepaRG cells (which, under controlled conditions, differentiate into both hepatocytes and cholangiocytes (Cerec et al., 2007)), primary human macrophages, and HSC-derived LX-2 cells. Given the presence of HepaRG cells, macrophages and LX-2 cells, we refer to this as the "HML" model. Our model reproduced the phenotypes of hepatocytes, cholangiocytes, HSCs, and Kupfer cells. We showed that the cells in 3D cultures of HML organoids remained in a differentiated state. When exposed to FAs, HML organoids exhibited the main features of NAFLD, namely steatosis, significant disturbance of phase 1 metabolism, fibrogenesis, and basal state inflammation. Furthermore, the HLM model was used to (i) evaluate drug toxicity in the presence or absence of NAFLD-like conditions and (ii) estimate the IC_{50} and the benchmark dose (BMD) in accordance with the guidelines issued by the European Food Safety Authority (EFSA Scientific Committee et al., 2017; Vieira Silva et al., 2021). Our results are in line with the clinical data in the literature and highlight the NAFLD-HML model's relevance for the early detection of at-risk drugs in patients with NAFLD.

2. Material and methods

2.1. Cell culture

Human HepaRG cells were cultured as described previously (Aninat, 2005). Progenitor HepaRG cells were seeded at a density of 2×10^6 cells in a 75 cm^2 flask in William's E culture medium (1×) supplemented with 10% foetal bovine serum (FBS), 2 mM glutamine, 50 μM sodium hydrocortisone hemisuccinate, 5 μg/mL insulin, 50 U/mL penicillin, and 50 μg/mL streptomycin. Starting two weeks after seeding, the cells were cultured for two additional weeks in the same medium supplemented with 2% DMSO; this resulted in differentiation into both cholangiocyte- and hepatocyte-like cell populations (Aninat, 2005; Cerec et al., 2007).

Human macrophages were differentiated from peripheral blood mononuclear cells, as described previously (Gicquel et al., 2015). The peripheral blood mononuclear cells were isolated by differential centrifugation on UNI-SEP U-10 (Novamed, Jerusalem, Israel) from buffy coat donations (from the French Blood Agency (*Etablissement Français du Sang*), Rennes, France). The experiments were performed in compliance with the French legislation on blood donation and blood product use and safety. Monocytes were enriched using a human CD14 separation kit (Microbeads; MiltenyiBiotec, Bergisch Gladbach, Germany), plated at a density of 4×10^6 cells in a 25 cm^2 flask, and cultured at 37 °C in RPMI 1640 medium supplemented with 100 IU/mL penicillin–100 mg/mL streptomycin, 2 mM L-glutamine, 1 mM HEPES and 10% FBS. Macrophages were obtained after differentiation from monocytes through incubation in RPMI medium with 50 ng/mL granulocyte-macrophage colony-stimulating factor for 7 days.

LX2 cells were provided by S.L. Friedman (Icahn School of Medicine at Mount Sinai, New York, NY, USA) and were cultured in the activated state in Dulbecco's Modified Eagle Medium supplemented with GlutaMAX™, pyruvate, 10% FBS, 50 U/mL penicillin, and 50 μg/mL streptomycin, as described previously (Schinagl et al., 2021; Xu et al., 2005).

2.2. Production of HML organoids

The HML organoids were obtained by seeding a solution of isolated cells in the Sigma micromold system (Z764051-6EA; Sigma Aldrich, St. Louis, MO, USA), as described previously (Messner et al., 2019). The mixed cells (80% differentiated-HepaRG cells, 10% macrophages, and 10% LX-2 cells) were seeded at a density of 2000 cells per organoid. In order to optimize the organoids' viability, the relative proportions of the cell types were optimized in preliminary experiments and were similar to those observed in a healthy liver. The self-assembly medium was composed of William's E medium supplemented with 10% FBS, 2 mM glutamine, 50 μM sodium hydrocortisone hemisuccinate, 5 μg/mL insulin, 50 U/mL penicillin, and 50 μg/mL streptomycin. After three days of culture, the FBS level was reduced to 1%, and HML organoids were cultured until 14 days after seeding.

2.3. Induction of steatosis and fibrosis

The HML organoids were treated with FA mixtures to induce steatosis, as described previously (Ferron et al., 2021). The mixture was composed of 150 μM stearic acid and 300 μM oleic acid and was prepared with FA-free BSA. Treatments were initiated on day (D) 5 after seeding and repeated every other day until D14.

2.4. Isolation of RNA and gene expression analysis

Total RNA was extracted with the Nucleospin RNA isolation kit (Macherey-Nagel, Düren, Germany) and then quantified using a Nanodrop 1000 system (Thermo Fisher Scientific, Waltham, MA, USA). Next, the RNAs were reverse-transcribed into cDNA, using the High-Capacity cDNA Reverse Transcription Kit (Applied Biosystems, Woolston, United Kingdom). Gene expression was assessed using real-time quantitative PCR analysis (RT-qPCR) with SYBR Green PCR Master Mix (Applied Biosystems, Woolston United Kingdom) and a 384-well QuantStudio™ 7 Flex Real-Time PCR System (Thermo Fisher Scientific). The sequences of the primers used to measure gene expression are given in Supplementary Table 1. The gene coding for alpha-1-microglobulin (*AMBP*) was chosen as the reference in expression experiments, and the relative RNA expression of each target gene was calculated using the $2^{-\Delta\Delta Ct}$ method.

2.5. Histochemical and immunohistochemical staining

HML organoids were harvested, fixed in 5% formalin for 60 min, and washed in PBS. After the organoids had been embedded in paraffin, blocks were cut into 4 μm slices. The latter were mounted on positively charged slides and dried at 58 °C for 60 min. Each slide was stained with hemalun-eosin-saffron (HES) reagent, in order to select the best slices prior to immunohistochemical staining. Immunohistochemical staining was performed on the Discovery ULTRA automated immunohistochemical stainer (Roche) using the Ventana detection kit (Ventana Medical Systems, Tucson, AZ, USA). Organoids were labelled using two combinations of antibodies: (i) rabbit anti-CYP3A4 (AB1254, Millipore), mouse anti-cytokeratin 19 (CK19) (clone RCK108, M0888,Dako), and mouse anti-CD68 (PG-M1) (MA5–12407, Invitrogen); and (ii) rabbit anti-Col1A1 (ab34710, Abcam), mouse anti-COL4 (Clone CIV22, M0785, Dako), and mouse anti-vimentin (V9-(3)) (M0725, Dako). Nuclei were stained with DAPI reagent and the slides were scanned on a PANNORAMIC confocal scanner (3DHISTECH Ltd., Budapest, Hungary)

at a magnification of 20×.

2.6. Image analysis

The acquired images were converted into the TIFF format and then analyzed using Qupath software version 0.43 (Bankhead et al., 2017). Nuclei were segmented using the StarDist extension (Schmidt et al., 2018). In immunofluorescence assays, a Qupath object classifier was used to identify and count the number of cells positive for CYP3A4, CK19, CD68 and/or vimentin per organoid for each condition. To assess fibrosis in each organoid, the total COL1 intensity was quantified and then calculated per nucleus.

2.7. Lipid extraction and FA analysis

Total lipids were extracted from 140 pooled organoids (~280,000 cells). The organoids were extracted twice with 2 mL of hexane/isopropanol (3/2 *v*/v) after acidification with 1 mL HCl 3 M and the addition of 2 μg heptadecanoic acid (C17:0, used as an internal standard for the quantification of FAs, as described previously (Lemarié et al., 2016). The cell lipids were then saponified for 15 min at 70 °C, using 1 mL of 0.5 M NaOH in methanol. After acidification with 1 mL HCl 3 M, the released free FAs were extracted twice with 2 mL diethyl ether. Samples were derivatized at room temperature for 15 min with 100 μL of 7% pentafluorobenzyl (PFB)-bromide in acetonitrile plus 10 μL of triethylamine (Kuiper et al., 2018). The solvents were removed under a stream of N_2, and the FA PFB-esters were resolubilized in 100 μL of hexane.

A very sensitive negative ion chemical ionization (NICI) gas chromatography–mass spectrometry (GC–MS) method was applied because the samples contained very small amounts of FAs. The analysis was carried out on a 7890 A GC system coupled to a 5977B MS detector (Agilent Technologies, Les Ulis, France). The PFB esters were injected in splitless mode onto a bonded silica capillary column (BPX 70, 60 m × 0.25 mm; SGE, Melbourne, Australia) containing a 70% cyanopropyl polysilphenylene-siloxane polar stationary phase (film thickness: 0.25 μm). Helium was used as the carrier gas (mean linear flow rate: 36 cm/s). The column temperature (initially 190 °C) was ramped up gradually (by 4 °C/min) to 250 °C and held there for 10 min. The transfer line, source and quadrupole temperatures were 280 °C, 200 °C and 150 °C, respectively. The mass spectrometer was operated in NICI mode using methane as the ionization gas, with a pressure of 1.5×10^{-4} Torr. Data were obtained in full scan mode, with a mass range of m/z 50–600 amu.

Fatty acids were identified on the basis of their retention time (R_t) *vs.* authentic standards and the corresponding specific [M-PFB] ion formed in the source. The peak area was integrated using MassHunter Workstation Software Qualitative Analysis (version B.07.00 for Windows, Agilent Technologies) (Guillocheau et al., 2019). Results were expressed as the mass of FAs divided by the cell count, after normalization against the area of the C17:0 internal standard.

2.8. Lipid staining and imaging

Organoids were harvested and incubated in a solution of 1 μM BODIPY™ 493/503 (Invitrogen) diluted in PBS for 30 min at 37 °C, prior to fixation in 5% formalin. Stained organoids were mounted on a glass slide and imaged on a Leica DMI6000 Inverted Microscope with a Yokogawa CSU-X1 Spinning Disk Head and driven by Inscoper Imaging Suite (Inscoper, Cesson Sevigné, France). Images were captured at a magnification of 20× and analyzed using ImageJ FIJI software (version 1.53). Total BODIPY™ intensity was quantified for each organoid and compared with the control conditions.

2.9. Quantification of secreted cytokines

The concentrations of interleukin IL1b, IL6, and transforming growth factor beta (TGF-β) in the medium were measured using Duoset ELISA kits (R&D Systems, Abingdon, United Kingdom). Apo-B secretion was measured using the Human Apolipoprotein-B ELISA pro kit (Mabtech, Nacka Strand, Sweden). Both ELISA kits were used according to the manufacturer's instructions.

2.10. Treatments with drug compounds

5-Fluorouracil, carbofuran, and valproate were purchased from Tokyo Chemical Industry Co., Ltd. (Tokyo, Japan). Paracetamol, troglitazone and voriconazole were purchased from Sigma Aldrich. Drugs were prepared in DMSO, and six serial ten-fold dilutions were prepared in culture medium. Troglitazone was tested at a maximal concentration of 0.2 mM, on the basis of published data (Allard et al., 2021; Bucher et al., 2018). Voriconazole, 5-fluorouracil and valproate were all tested at 2 mM, and acetaminophen was tested at 20 mM; this gave concentrations close to 100× the C_{max} published in the literature (Lazarus et al., 2002; Porceddu et al., 2012; Wy et al., 2007). To evaluate drug toxicity, HML organoids were generated in 96-well round bottom ultra-low attachment plates. Briefly, 2000 cells were seeded per well, with the cell ratio (80% HepaRG cells, 10% macrophages, and 10% LX-2 cells) and culture conditions described above. On D5, 80% of the well medium was renewed with free medium containing the compounds prepared in 0.5% DMSO. The medium was again renewed on D7, D10, D12 and D14, prior to the measurement of the intracellular level of ATP.

2.11. Measurement of intracellular ATP

The intracellular level of ATP was measured using the CellTiter-Glo® Luminescent Cell Viability assay (Promega, Charbonnières, France). In line with the manufacturer's instructions, control and treated organoids were incubated with the CellTiter-Glo® reagent for 10 min at room temperature. Cell lysates were then transferred to white multiwell plates, and the luminescence signal was quantified using a POLARstar Omega microplate reader (BMG Labtech, Ortenberg, Germany). The results were expressed as a percentage of the control value, and IC_{50} values were calculated using GraphPad Prism software (version 8, GraphPad Inc., La Jolla, CA, USA) with the same sigmoidal dose-response regression model applied to each compound.

2.12. Determination of the BMD

The viability data were evaluated quantitatively in a BMD analysis, using the PROAST package in R software (version 66.20) on the EFSA's website (https://r4eu.efsa.europa.eu/app/bmd) and in line with the corresponding technical guidance (EFSA Scientific Committee et al., 2017). Based on the interpolation of a fitted dose-response model, the BMD approach estimates the dose associated with a small effect size. The BMD was estimated for a benchmark response of 5% and was reported as the lower confidence bound. The confidence interval for the lower bound was estimated using parametric bootstrap sampling (Table 1). Lastly, the BMD estimated from the viability assay data was used to rank the compounds by potency.

2.13. Statistical analysis

Unless stated otherwise, all data are quoted as the mean ± standard deviation (SD). The threshold for statistical significance was set to $p < 0.05$. All experiments were performed independently at least three times. All statistical analyses were performed using GraphPad Prism software (version 8) and paired two-tailed Student's *t*-tests.

Table 1
Estimated IC_{50} value and BMDs for HepaRG cells and HML organoids exposed to drugs. The BMD was modelled using the PROAST package in R software, and the IC_{50} was estimated using GraphPad Prism software. The results are expressed as mean values. FA-exposed conditions and control (CTL) experiments were compared in a paired *t*-test (*$p \leq 0.05$).

		HepaRG cells				HML organoids			
		IC_{50} (μM)		BMD (μM)		IC_{50} (μM)		BMD (μM)	
	C_{max}	CTL	FA	CTL	FA	CTL	FA	CTL	FA
5-FU	1	497	**952***	101	169	279	931	49	201
Paracetamol	199	1131	1407	227	502	5005	**725***	1457	287
Valproate	1005	2330	2458	441	529	772	863	190	277
Voriconazole	3	1144	1135	380	468	67	48	79	26
Troglitazone	2	84	90	56	41	127	**31***	28	10

3. Results

3.1. HML organoids express liver cell markers

HML organoids were harvested on D5, D7, D10 and D14 of culture and analyzed histologically (Fig. 1). HES staining (Fig. 1A) showed that the cells had a segregated organization in the organoid. The organoid's diameter ranged from 200 to 300 μm, and a necrotic area in the centre of the organoid was never observed. CYP3A4 immunohistochemical staining (Fig. 1B) showed that typical, large, polygonal hepatocytes were distributed throughout the organoids. Staining for the epithelial marker cytokeratin 19 (CK19) highlighted the presence of cholangiocyte-like cells, which were mostly in the outer region of the organoids. The quantification of CYP3A4- and CK19-positive cells (Fig. 2A) showed that the number of HepaRG cells within the organoid remained stable over the 14-day culture period – albeit with a small (non-significant) decrease at D7. The stellate cells (revealed by vimentin staining) self-organized over the 14-day culture period and spread over the outside of the organoids (Fig. 1C). The quantification of CD68-positive cells revealed that the M1 macrophages in the organoids remained differentiated throughout the culture period (Fig. 1B). These results were confirmed quantitative image analysis of the CD68- and

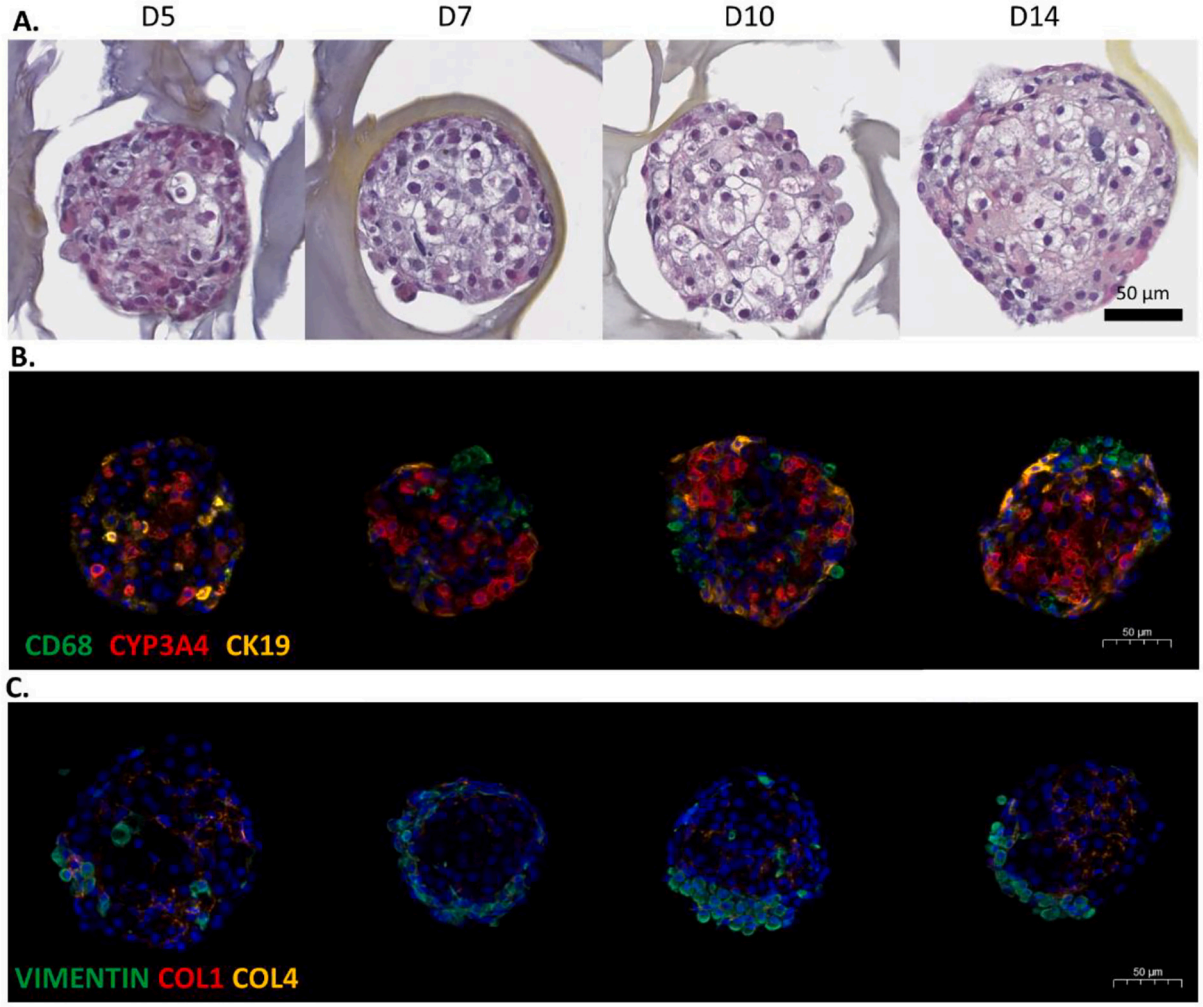

Fig. 1. Characterization of the HML organoid culture. HML organoids were collected at D5, D7, D10, and D14 after seeding, fixed in 5% paraformaldehyde, embedded in paraffin, and processed for immunohistochemical analysis. (A) HML organoids were stained with hemalun–eosin–saffron (HES). (B and C) HML organoids were stained using (i) anti-CD68, anti-CYP3A4 and anti-CK19 antibodies, and (ii) anti-vimentin, anti-COL1A1 and anti-COL4 antibodies.

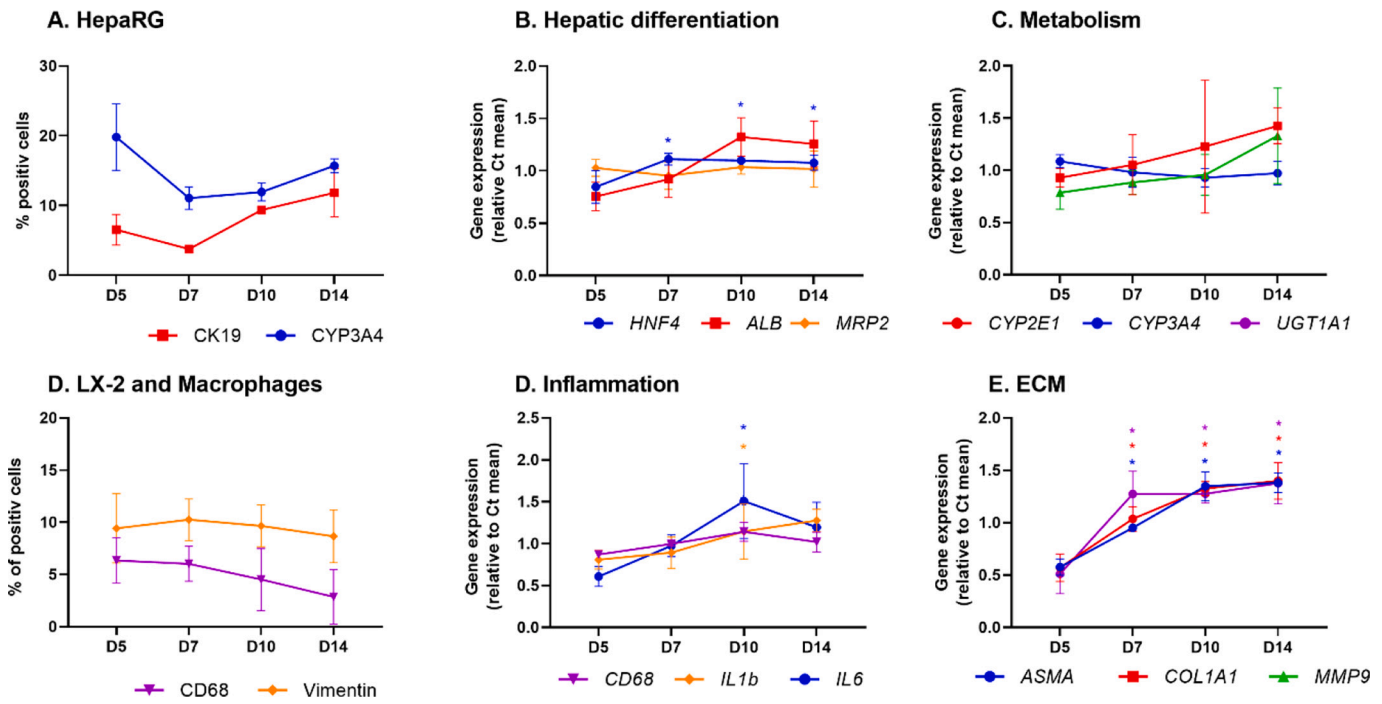

Fig. 2. Changes over time in the expression of cell markers in HML organoids cultured for 5 to 14 days, based on RT-qPCR assays of total RNA and image analysis. (A and D) HML organoids were harvested at D5, D7, D10 and D14. The protein and gene expression levels of several markers of hepatocytes, cholangiocytes, macrophages and stellate cells were then measured. The images shown in Fig. 1 were analyzed using Qupath, in order to estimate the number of cells positive for CK19, CYP3A4, CD68 and/or vimentin per organoid. (B. C. D. and E) RT-qPCR assays were used to assess the expression of the genes coding for *HNF4, ALB, UGT1A1, MRP2, CYP3A4, CYP2E1, A-SMA, CD68, COL1A1, IL1b, IL6* and *MMP9*. These gene expression data were normalized against the level of *AMBP* expression ($2^{-\Delta\Delta Ct}$) ± SD and expressed relative to the average expression of each marker. *$p \leq 0.05$ in a paired *t*-test, based on data from three independent experiments.

vimentin-positive cells positive (Fig. 2D). Collagen 1 and 4 (COL1 and COL4) deposits in the organoid remained scarce on D14 (Fig. 1C).

3.2. HML organoids maintain the expression of differentiation markers and upregulate the expression of xenobiotic-metabolizing enzymes

Our gene expression analysis of HML organoids showed that hepatic markers hepatocyte nuclear factor-4 alpha (HNF4α) and albumin were slightly upregulated between D7 and D10 and between D5 and D7, respectively; expression remained high until D14 (Fig. 2B). The expression levels of the phase 1 and 2 xenobiotic metabolizing enzymes CYP2E1, CYP3A4 and UGT1A1 increased over time (Fig. 2C), as previously observed in HepaRG spheroids (Gunness et al., 2013). The expression of the Phase 3 transporter MRP2 was stable over the 14-day culture period and appeared to be correlated with the polarization of the cholangiocyte apical membrane (as evidenced by CK19 labelling) and the hepatocyte canalicular membrane. Stellate cells (as evidenced by A-SMA and COL1A1 labelling) and M1 macrophages (CD68) were maintained from D5 to D14 (Fig. 2D and E). Although levels of IL6 and MMP9 gene expression increased over time, the Ct values were low; this revealed a potential change in the ECM and a low basal state of inflammation in the HML organoids.

3.3. An FA mixture induces steatosis in HML organoids

HML organoids were exposed to an FA mixture (150 μM stearic acid (C18:0) and 300 μM oleic acid (C18:1 n-9)) from D5 to D14. Lipid labelling (Fig. 3A) showed that exposure to the FA mixture was associated with an increase in the quantity of neutral lipid droplets in the treated organoids after 9 days of exposure. BODIPY™ staining and the total TG content were higher in FA-treated organoids than in controls (Fig. 3B). An in-depth GC–MS analysis of the FA composition of total lipids (Fig. 3C) reveals that control HML organoids were mainly composed of saturated FAs (C16:0, C18:0, C14:0) and monounsaturated FAs (C18:1 n-9, C18:1 n-7, C16:1 n-7), with low amounts of polyunsaturated FAs in general and n-3 FAs in particular. When treated with the mixture of C18:0/C18:1 n-9, the organoids accumulated C18:1 n-9 significantly more than other FAs (relative to controls) such as C18:0, the latter FA was probably Δ9-desaturated rapidly after its uptake by the cells, thus further increasing the amount of C18:1 n-9.

3.4. Fatty-acid-treated HML organoids present features of NAFLD

Organoids exposed to FA for 9 days presented several characteristics of NAFLD (Fig. 4). The FA treatment was associated with greater production of COL1 and COL4 in the organoids (Fig. 4A), together with fibrosis (as quantified by image analysis; Fig. 4B). The level of CYP3A4 gene expression was significantly lower in FA-treated HML organoids, and that of COL1A1 was significantly higher (Fig. 4C). HML organoids exposed to FA also displayed a significantly higher levels of CYP2E1 and UGT1A1 expression, compared with controls. The expression of lipid-metabolism-related genes (such as lipid droplet coating protein perilipin 2 (PLIN2) and apolipoprotein B (APOB) gene (Fig. 4C)) and levels of protein secretion (Fig. 4D) were significantly higher in FA-exposed HML organoids; these are characteristics of the onset of liver steatosis (Wang et al., 2020). HML organoids treated with FA secreted greater amounts of the pro-inflammatory cytokines IL1b and IL6 and the pro-fibrotic cytokine TGF-β, in line with the results of the gene expression assays (Fig. 4C and D). Although we observed greater expression of the pro-inflammatory cytokine IL6, the levels of TNFA gene expression were similar in the control and FA conditions. These results evidenced the major physiological changes in xenobiotic and lipid metabolism induced by FA exposure of HML organoids - changes that recapitulate the main features of NAFLD.

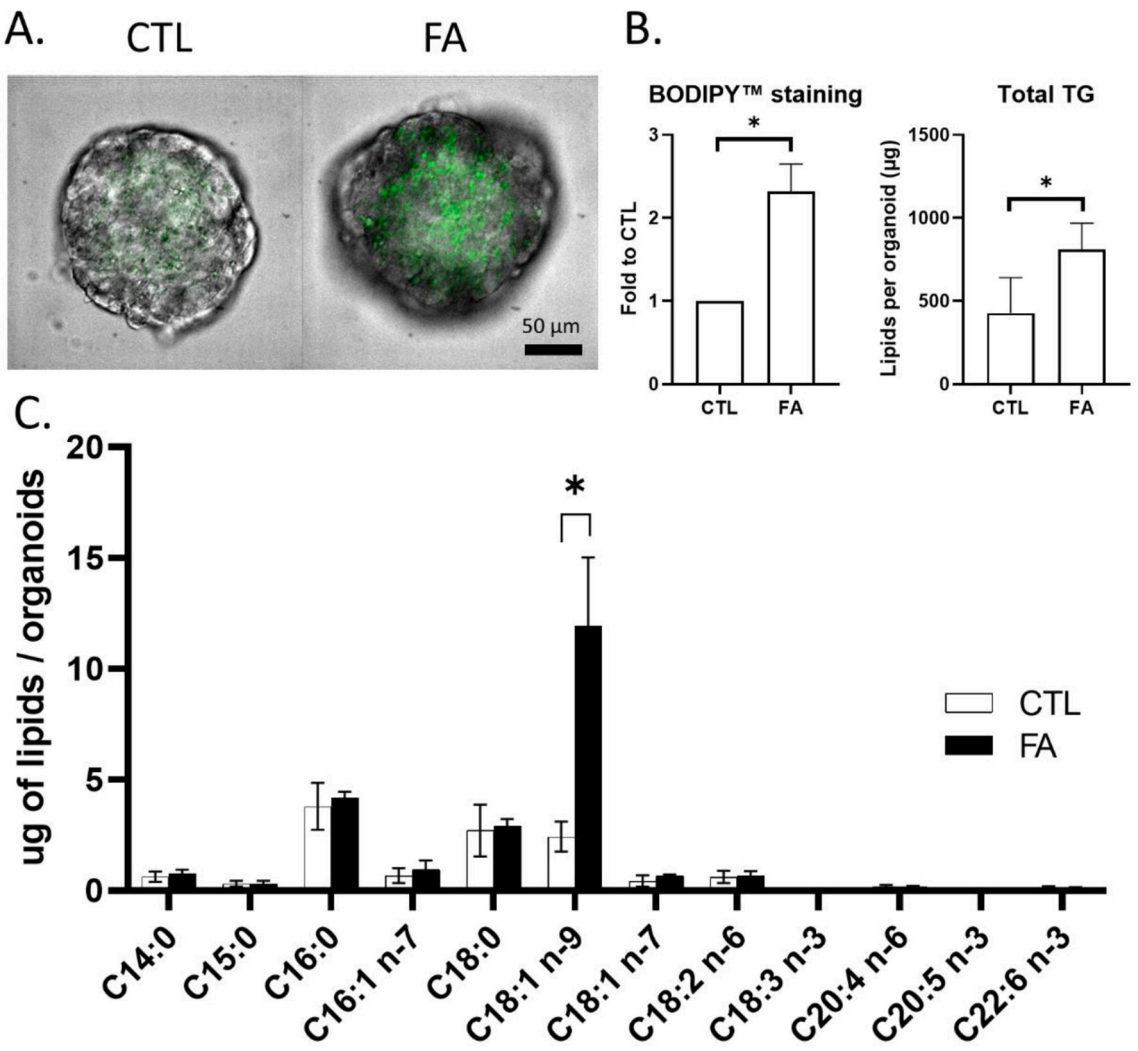

Fig. 3. Induction of steatosis in HML organoids through exposure to an FA mixture. HML organoids were exposed to a mixture of stearic acid and oleic acid from D5 to D14 of culture, before harvesting and lipidomic analysis. (A) HML organoids stained with BODIPY™ and imaged at a magnification of 20×. (B) GC–MS quantification of total TGs and BODIPY™ staining in HML organoids. C. GC–MS lipidomic analysis of HML organoids. *$p \leq 0.05$, determined in a paired t-test (relative to control (CTL) experiments) and based on data from three independent experiments.

3.5. Evaluation of drug cytotoxicity in NAFLD organoids

We used FA-exposed HML organoids and differentiated HepaRG monolayer cells to evaluate the impact of NAFLD in drug cytotoxicity. The tested drugs were chosen on the basis of their mode of action and known hepatoxicity: 5-FU, a uracil analogue used as antimetabolite in the treatment of various cancers; acetaminophen, an analgesic which primarily causes hepatotoxicity through reactive metabolite formation; valproate, an antiepileptic drug that blocks voltage-gated sodium channels; voriconazole, an antifungal triazole used to treat aspergillosis; and troglitazone, an antidiabetic drug withdrawn from the market and that causes beta oxidation of FAs and opening of the mitochondrial permeability transition pore. HepaRG cells and HML organoids were exposed to FAs from D5 to D14, and to drugs from D7 to D14. Cytotoxicity was evaluated using intracellular ATP measurements and dose-response modeling of the IC_{50} and BMD (Fig. 5 and Table 1).

Organoids cultured with FAs alone did not show signs of cytotoxicity, relative to organoids cultured under control conditions (data not shown). 5-FU was significantly less cytotoxic when differentiated HepaRG cells and HML organoids were exposed to FAs: the IC_{50} rose from 497 µM to 952 µM with HepaRG cells and from 279 µM to 931 µM with HML organoids. The relative reduction in the cytotoxicity of 5-FU in the presence of FAs was also demonstrated by a comparison of the respective BMDs. With HepaRG cells, exposure to FA did not appear to influence the IC_{50} values for valproate (2330 µM to 2458 µM in the absence and presence of FAs, respectively) or voriconazole (1144 µM and 1135 µM, respectively). Troglitazone was more toxic in HML organoids treated with FA; the IC_{50} rose from 127 µM to 131 µM, and the BMD fell from 28 µM to 10 µM. HepaRG cells exposed to FA were not more sensitive to paracetamol: the IC_{50} values were 1131 µM and 1407 µM in the absence and presence of FAs, respectively). In contrast, FA-exposed HML organoids were more sensitive to paracetamol, with IC_{50} values of 5005.0 µM and 725.2 µM in the absence and presence of FAs, respectively.

Based on the IC_{50} and BMD values, we evaluated the ability of differentiated HepaRG cells and HML organoids to evaluate the toxicity of 5-FU, paracetamol, valproate, voriconazole and troglitazone (relative to the corresponding C_{max}; Fig. 6). A regression analysis of the relationship between C_{max} and IC_{50} or BMD is shown in Fig. 6A. The IC_{50} and BMD values estimated with HML organoids were better correlated with the C_{max} than the values estimated with HepaRG cells. Moreover, the IC_{50} or BMD values under control conditions were more strongly correlated with Cmax than the values obtained under FA-exposed conditions. According to the relative potency factors for drug toxicity in the NAFLD condition *vs.* the control condition (Fig. 6B), the HML organoids were more sensitive to drugs (especially paracetamol and troglitazone) than the 2D differentiated HepaRG cells. However, differentiated

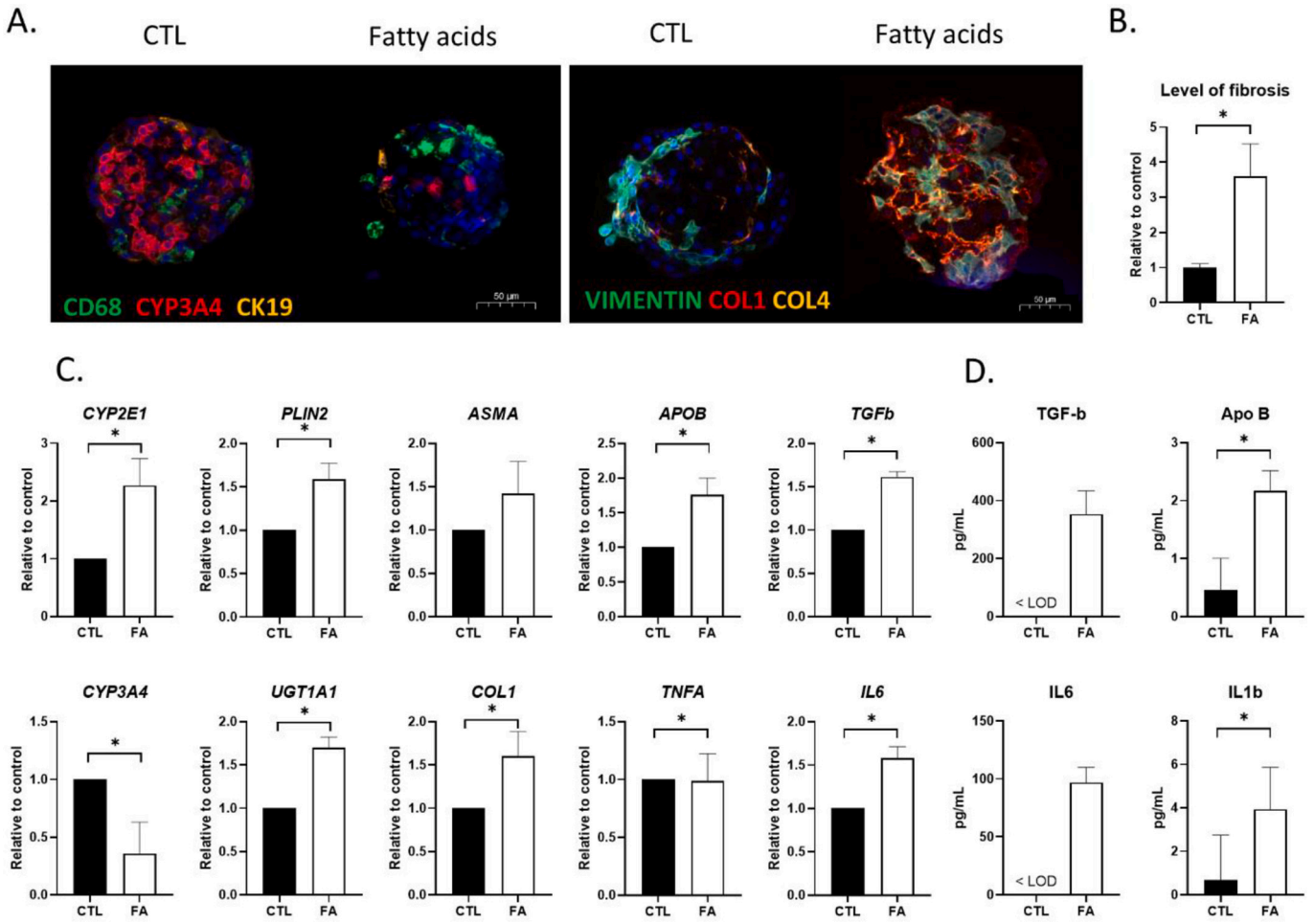

Fig. 4. Characteristics of NAFLD induced by the exposure of HML organoids to FAs. HML organoids were exposed to FAs from D5 to D14, prior to harvesting and immunohistochemical staining or gene expression analysis. (A) Control (CTL) organoids and FA-exposed organoids were embedded in paraffin and process for immunohistochemical labelling of CD68 (in green), CYP3A4 (in red) and CK19 (in yellow) in the left-hand panel and vimentin (in green), COL1 (in red) and COL4 (in yellow) in the right-hand panel. (B) Quantification of fibrosis in HML organoids, based on COL1 staining. (C) HML organoids were harvested at D14, prior to measurement of the expression of NAFLD marker genes. q-RT-PCR assays of total RNA were used to assess the expression of the *CYP2E1*, *CYP3A4*, *PLIN2*, *UGT1A1*, *ASMA*, *COL1*, *APOB*, *TNFA*, *TGFB* and *IL6* genes. The data are expressed as $2^{-\Delta\Delta Ct} \pm$ SD, relative to *AMBP*. (D) Levels of secreted IL1b, ApoB, IL6 and TGF-β in the culture supernatant, as measured in ELISAs. $^*p \leq 0.05$ in a paired *t*-test, based on data from three independent experiments. (For interpretation of the references to colour in this figure legend, the reader is referred to the web version of this article.)

HepaRG cells detected the cytotoxicity of valproate with greater sensitivity because the IC_{50} and BMD values were <10 times greater than the C_{max}.

4. Discussion

We were able to maintain liver functions *in vitro* (including the activity of phase 1 and 2 xenobiotic-metabolizing enzymes) in 2D co-cultures of adult pHHs with either biliary epithelial cells or HSCs (Fraslin et al., 1985). Interestingly, the HepaRG progenitor cell line can differentiate into both cholangiocyte-like and hepatocyte-like cells: both cell types then shown signs of liver-specific functions (Aninat et al., 2006). In order to reproduce immune-mediated hepatotoxicity and study the role of inflammatory stress in the idiosyncratic hepatotoxicity of diclofenac, macrophages and HepaRG have been co-cultured in two dimensions (Al-Attrache et al., 2016). HepaRG cells have been co-cultured with primary HSCs in three dimensions, in order to investigate liver fibrosis (Leite et al., 2016). In the present study, we established an HML 3D liver organoid model system by mixing four cell types: differentiated HepaRG hepatocyte-like and cholangiocyte-like cells, HSC-derived LX-2 cells, and macrophages. Furthermore, we established a NAFLD-like state in the HML model and demonstrated that these organoids could detect drug hepatotoxicity in this context.

We firstly showed that HepaRG, LX-2 and macrophages can be cocultured in 3D in DMSO-free and low-FBS conditions. In HML organoids, differentiated HepaRG cells express markers of both hepatocyte and cholangiocytes, together with those of HSCs and immune cells. Furthermore, high expression levels of genes involved in phase 1 and 2 xenobiotic metabolism were observed in HML organoids. The stable, high levels of liver markers expression until D14 of culture enabled us to perform chronic exposure studies. Although previously developed 3D *in vitro* systems based on HepaRG cells also expressed high levels of xenobiotic-metabolizing enzymes under DMSO-free conditions (Rose et al., 2021), they were cultured in a collagen matrix and did not include other hepatic cell types. More recently, HepaRG cells were 3D co-cultured with THP-1 monocytes and immortalized HSCs, in order to model the fibrotic phenotype (Yan et al., 2021). Here, we used primary human monocytes as a source of macrophages, since THP-1 cells are highly proliferative (Chanput et al., 2014). We also developed a pathologically relevant NAFLD model using a mixture of stearic and oleic acids; this mixture reportedly increased lipid accumulation and metabolic dysfunction in HepaRG cells (Bucher et al., 2018). In HML organoids, FA treatment was associated with greater TG accumulation and the appearance of mild inflammatory and pro-fibrotic responses that

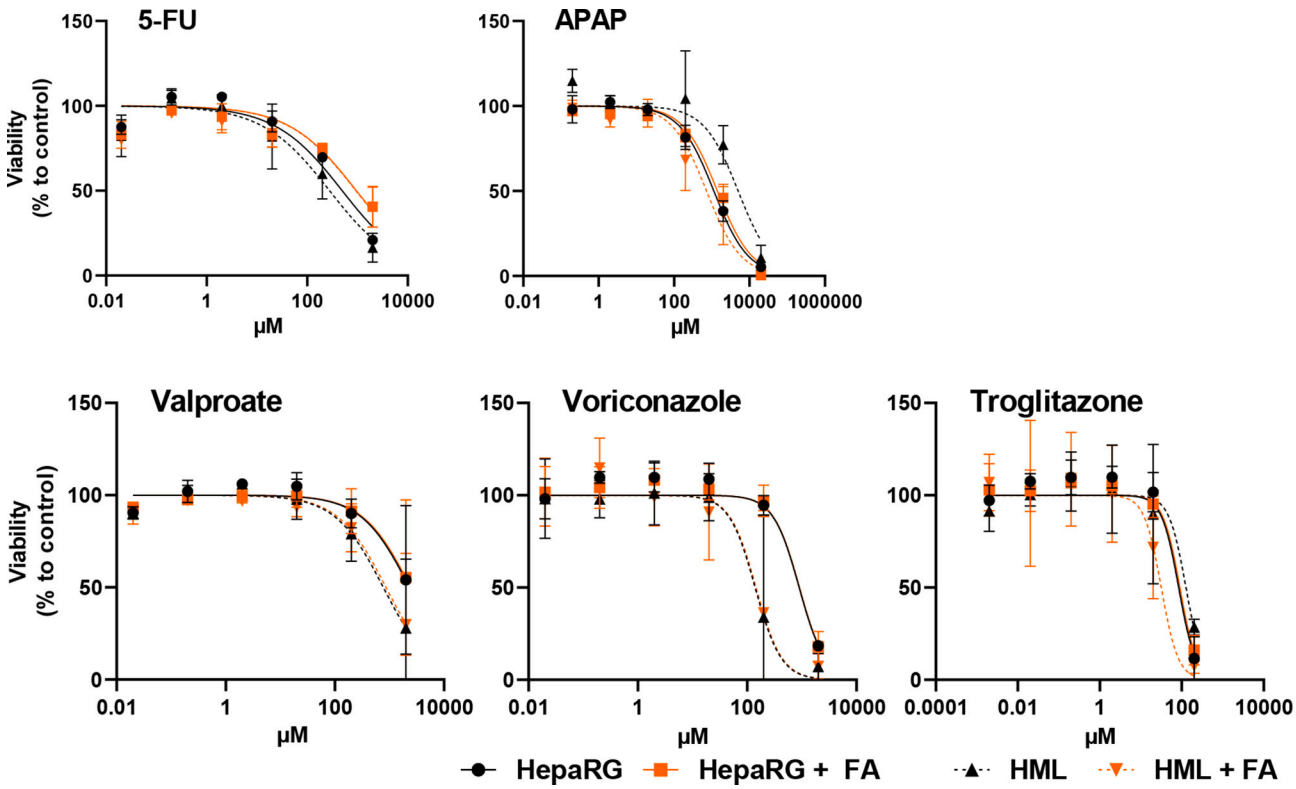

Fig. 5. Evaluation of drug toxicity on steatotic HepaRG cells and HML organoids, after 9 days of exposure. HepaRG cells and HML organoids were exposed to a mixture of FAs on D5. Next, 5-fluorouracil (5-FU), paracetamol, valproate, voriconazole or troglitazone was added to the medium from D7 to D14. Toxicity was assessed by measurement of the intracellular level of ATP. Using data from three independent experiments, the dose-response curves were modelled using the Hill slope function in GraphPad Prism software.

recapitulated the features of steatohepatitis. Oleic acid (taken up directly from the culture medium and also synthesized through the Δ9-desaturation of stearic acid) accumulated in TGs, which were stored as lipid droplets in the organoids. Treatment with stearic acid and oleic acid was associated with lower expression of the phase 1 xenobiotic metabolizing enzyme CYP3A4 and greater expression of CYP2E1 and phase 2 UGT1A1, as also reported in clinical and preclinical studies of NAFLD (Aubert et al., 2011; Michaut et al., 2016). Thus, our data suggest that the HML organoid is a relevant model of NAFLD.

Several clinical investigations have shown that obesity and NAFLD favour DILI in patients treated with various drugs (including omeprazole, telithromycin, and halothane (Massart et al., 2017; Tarantino et al., 2007)) and in individuals intoxicated with high doses of paracetamol (Begriche et al., 2023; Chomchai and Chomchai, 2018). Studies of obese rodents with NAFLD showed that acute treatments of high doses of paracetamol were more hepatotoxic than in lean (control) animals (Aubert et al., 2012; Begriche et al., 2023). It is noteworthy that the more severe paracetamol-induced liver injury observed in patients with NAFLD and in experimental NAFLD is thought to be related to higher levels of CYP2E1 activity, although other mechanisms might additionally be involved (Begriche et al., 2023; Michaut et al., 2014). More recently, we showed that acute paracetamol treatment was more cytotoxic in fat-laden, differentiated HepaRG cells than in control HepaRG cells; this was also due to higher levels of CYP2E1 activity in this cellular model of NAFLD (Michaut et al., 2016). To the best of our knowledge, however, the effect of repeated paracetamol treatments in steatotic HepaRG cells has not previously been investigated. In the present study, we showed for the first time that repeated paracetamol exposure was significantly more cytotoxic in NAFLD-HML organoids than in control HML organoids, whereas there was no difference in the cytotoxic effects on steatotic HepaRG cells *vs.* control HepaRG cells. Hence, our results highlight the need for further investigations of the hepatoxicity of repeated or chronic paracetamol exposure in obese patients with NAFLD. Indeed, obesity is one of the main risk factors for chronic diseases associated with persistent pain (such as osteoarthritis and low back pain) and that are typically treated with repeated doses of analgesic drugs - including paracetamol (Ambrosio et al., 2023; Conaghan et al., 2019).

Our results also showed that repeated treatment with troglitazone was significantly more cytotoxic in NAFLD-HML organoids than in control HML organoids, whereas there was no difference between steatotic and control HepaRG cells in a 2D culture. In previous research, we showed that troglitazone was moderately but significantly more cytotoxic in steatotic HepaRG cells (IC_{50}: 70 μM) than in non-steatotic cells (IC_{50}: 59 μM) (Le Guillou et al., 2018). It should be noted that the duration of FA and troglitazone exposure was 14 days in our first study (Le Guillou et al., 2018)) and only 7 days in the present study. Nevertheless, our present results indicate that greater cytotoxicity of troglitazone was observed in NAFLD-HML organoids (but not in differentiated HepaRG cells in a 2D culture) after 7 days of exposure. The greater cytotoxicity of troglitazone in steatotic HepaRG cells might be due to less biotransformation of this drug *via* the CYP3A4 pathway (Le Guillou et al., 2018). The same mechanism might operate in NAFLD-HML organoids, which also presented lower levels of CYP3A4 expression. The relatively high incidence of severe liver failure in troglitazone-treated patients with type 2 diabetes might be due (at least in part) to the presence of NAFLD in these individuals (Le Guillou et al., 2018). Unfortunately, it will not be possible to test this hypothesis prospectively in the clinic because this thiazolidinedione derivative was withdrawn from the market in 2000 in Japan and the US, due to unacceptable levels of hepatotoxicity (Ikeda, 2011; Massart et al., 2022).

Conversely, we found that the antineoplastic drug 5-FU was less cytotoxic in the context of FA exposure, although this was only statistically significant for steatotic HepaRG cells. 5-FU is rather well-

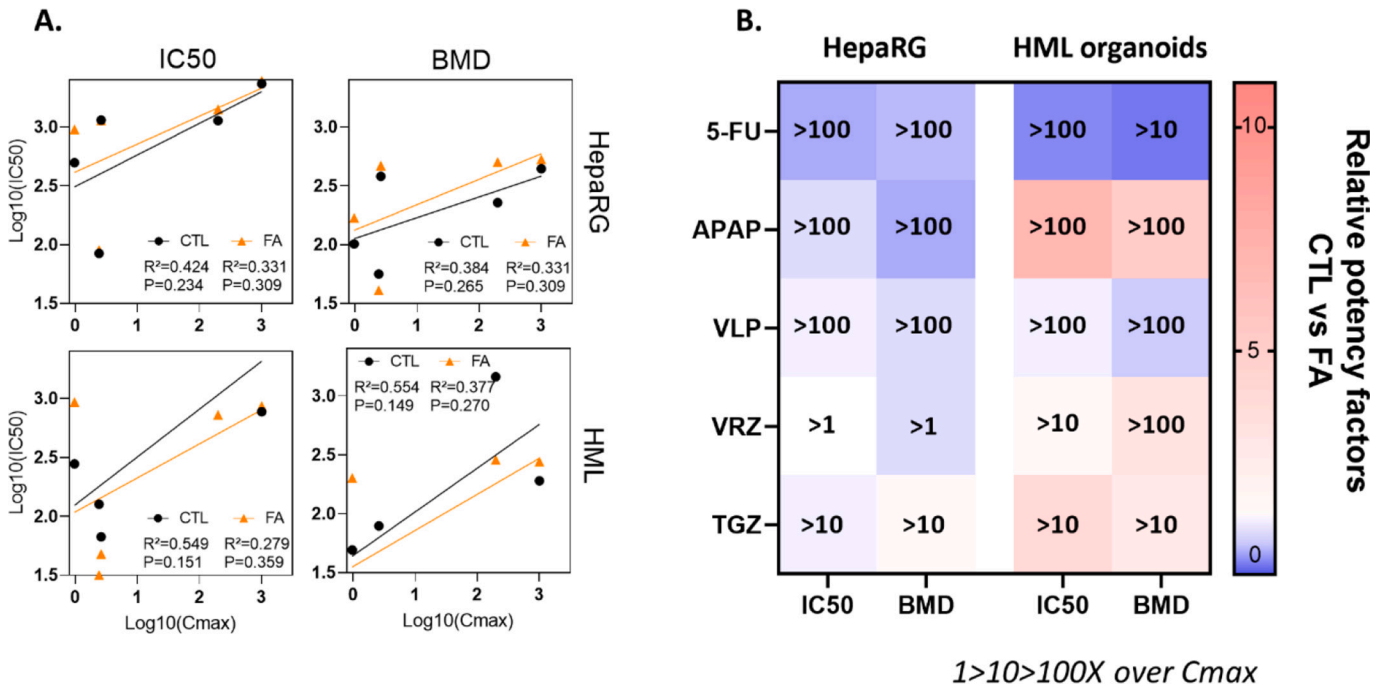

Fig. 6. Analysis of the ability of HepaRG cells and HML organoids to detect drug toxicity, as a model of NAFLD. (A) Regression analysis of the relationship between IC_{50} or BMD values with C_{max}. Black and yellow points represent values for 5-fluorouracil (5-FU), paracetamol, valproate (VLP), voriconazole (VRZ) and troglitazone (TGZ) measured in the presence or absence of FAs, respectively. The regression metrics are indicated on the graphs. (B) A heatmap summarizing the relative potency factors of drugs and conditions tested with HepaRG cells and HML organoids, relative to the control condition. The data are presented as IC_{50} and BMD values for FA treatments and are normalized against the control condition. The IC_{50} and BMD values were compared with C_{max} and plotted on a graph as fold-values in the following classes: ">1 C_{max}", ">10 C_{max}" and ">100 C_{max}". The C_{max} values were obtained from the literature: 0.96 μM for 5-FU (Wy et al., 2007), 196 μM for paracetamol (French public data base of drugs, 2022); 1005 μM for valproate (FDA, 1996), 2.5 μM for voriconazole (Lazarus et al., 2002), and 2.4 μM for troglitazone (FDA, 1999). (For interpretation of the references to colour in this figure legend, the reader is referred to the web version of this article.)

tolerated; although elevation of the liver enzymes aspartate transaminase and alanine transaminase occurs in up to 70% of treated patients, this phenomenon is usually mild and transient (Yaegashi et al., 2020). Hence, our data suggest that obese patients with preexisting NAFLD might have a lower risk of 5-FU-induced hepatic cytolysis. Further investigations are required to confirm this hypothesis. Notably, 5-FU toxicity is favoured by deficiencies in dihydropyrimidine dehydrogenase (DPYD), the initial (and rate-limiting) enzyme in 5-FU catabolism (van Kuilenburg, 2004). However, data from microarray experiments on HepaRG cells (GSE102536 https://www.ncbi.nlm.nih.gov/geo/query/acc.cgi?acc=GSE102536) showed that DPYD expression was similar in steatotic and non-steatotic conditions, whereas CYP2E1 expression was higher in steatotic cells and CYP3A4 expression was lower (Bucher et al., 2018). Similarly, mRNA expression levels of DPYD were similar in FA-treated and control pHHs; in contrast, expression levels of various genes related to metabolic homeostasis were higher in FA-treated pHHs (Sullivan et al., 2022). Hence, further mechanistic investigations are needed so that we can understand why 5-FU is less cytotoxic in steatotic HepaRG cells and HML organoids and establish whether this observation could be translated into the clinic.

Lastly, our present results show that the antifungal voriconazole and the antiepileptic valproate had the same cytotoxic potential in steatotic and non-steatotic HepaRG cells and HML organoids. These data are in line with the assumption that some drugs are not more hepatotoxic in obese patients with NAFLD (Massart et al., 2017). For instance, several clinical studies have shown that hypolipidemic statins are safe for the liver in NAFLD (Massart and Fromenty, 2017; Nascimbeni et al., 2019). Hence, our NAFLD models in HepaRG cells and HML organoids might be invaluable for screening a large number of drugs and determining which might be more toxic in people with NAFLD. Any drugs identified in this way could be investigated further in rodent models of NAFLD and in prospective clinical studies (Allard et al., 2019).

In conclusion, we established a robust 3D *in vitro* liver organoid model using HepaRG hepatocyte- and cholangiocyte-like cells, LX-2 cells, and human primary macrophages. All the cell types remained differentiated and functional during the culture period. Importantly, an NAFLD-like state can be reliably induced in the HML organoid model and might therefore be relevant for *in vitro* drug screening and mechanistic studies of adverse outcome pathways in NAFLD/MASLD.

Author contributions

Conceptualization, PJF and BC; methodology PJF, JB, CS, AC and BF; cell culture, drug exposure, imaging, and lipid analysis, PJF, JB, RV, DC, VR and LM; data processing and analysis PJF, JB, DC, VR, AC and BF; the first draft of the manuscript was written by PJF, and all authors contributed to the manuscript. All authors read and approved the final manuscript.

Fundings

This work was funded by the Institut National de la Santé et de la Recherche Médicale (INSERM), the Centre National de la Recherche Scientifique (CNRS), the University of Rennes, and the French Agency for the Safety of Drugs and Health Products (ANSM), as part of the PREVITOX network project. Additional funding was received from the Brittany Regional Council, as part of the InnovCell 3D project.

Declaration of Competing Interest

The authors declare the following financial interests/personal relationships which may be considered as potential competing interests:

Ferron reports financial support was provided by National Agency for Safety of Medicines and Health Products.

Data availability

Data will be made available on request.

Acknowledgements

The authors thank Thierry Pécot (FAIIA Core Facility, UAR Biosit, Rennes, France) for help with the Qpath image analysis.

Appendix A. Supplementary data

Supplementary data to this article can be found online at https://doi.org/10.1016/j.tiv.2023.105728.

References

Al-Attrache, H., Sharanek, A., Burban, A., Burbank, M., Gicquel, T., Abdel-Razzak, Z., Guguen-Guillouzo, C., Morel, I., Guillouzo, A., 2016. Differential sensitivity of metabolically competent and non-competent HepaRG cells to apoptosis induced by diclofenac combined or not with TNF-α. Toxicol. Lett. 258, 71–86. https://doi.org/10.1016/j.toxlet.2016.06.008.

Allard, J., Le Guillou, D., Begriche, K., Fromenty, B., 2019. Drug-induced liver injury in obesity and nonalcoholic fatty liver disease. In: Advances in Pharmacology. Elsevier, pp. 75–107. https://doi.org/10.1016/bs.apha.2019.01.003.

Allard, J., Bucher, S., Massart, J., Ferron, P.-J., Le Guillou, D., Loyant, R., Daniel, Y., Launay, Y., Buron, N., Begriche, K., Borgne-Sanchez, A., Fromenty, B., 2021. Drug-induced hepatic steatosis in absence of severe mitochondrial dysfunction in HepaRG cells: proof of multiple mechanism-based toxicity. Cell Biol. Toxicol. 37, 151–175. https://doi.org/10.1007/s10565-020-09537-1.

Ambrosio, L., Mazzuca, G., Maguolo, A., Russo, F., Cannata, F., Vadalà, G., Maffeis, C., Papalia, R., Denaro, V., 2023. The burden of low back pain in children and adolescents with overweight and obesity: from pathophysiology to prevention and treatment strategies. Therap. Adv. Musculoskel. 15 https://doi.org/10.1177/1759720X231188831, 1759720X231188831.

Aninat, C., 2005. Expression of cytochromes P450, conjugatin enzymes and nuclear receptors in human hepatoma HepaRG cells. Drug Metab. Dispos. 34, 75–83. https://doi.org/10.1124/dmd.105.006759.

Aninat, C., Piton, A., Glaise, D., Charpentier, T.L., Langouët, S., Morel, F., Guguen-Guillouzo, C., Guillouzo, A., 2006. Expression of cytochromes P450, conjugating enzymes and nuclear receptors in human hepatoma HepaRG cells. Drug Metab. Dispos. 34, 75–83. https://doi.org/10.1124/dmd.105.006759.

Aubert, J., Begriche, K., Knockaert, L., Robin, M.A., Fromenty, B., 2011. Increased expression of cytochrome P450 2E1 in nonalcoholic fatty liver disease: mechanisms and pathophysiological role. Clin. Res. Hepatol. Gastroenterol. 35, 630–637. https://doi.org/10.1016/j.clinre.2011.04.015.

Aubert, J., Begriche, K., Delannoy, M., Morel, I., Pajaud, J., Ribault, C., Lepage, S., McGill, M.R., Lucas-Clerc, C., Turlin, B., Robin, M.-A., Jaeschke, H., Fromenty, B., 2012. Differences in early acetaminophen hepatotoxicity between obese *ob/ob* and *db/db* mice. J. Pharmacol. Exp. Ther. 342, 676–687. https://doi.org/10.1124/jpet.112.193813.

Bankhead, P., Loughrey, M.B., Fernández, J.A., Dombrowski, Y., McArt, D.G., Dunne, P. D., McQuaid, S., Gray, R.T., Murray, L.J., Coleman, H.G., James, J.A., Salto-Tellez, M., Hamilton, P.W., 2017. QuPath: open source software for digital pathology image analysis. Sci. Rep. 7, 16878. https://doi.org/10.1038/s41598-017-17204-5.

Barranger, A., Hégarat, L.L., 2022. Towards better prediction of xenobiotic genotoxicity: CometChip technology coupled with a 3D model of HepaRG human liver cells. Arch. Toxicol. https://doi.org/10.1007/s00204-022-03292-4.

Begriche, K., Penhoat, C., Bernabeu-Gentey, P., Massart, J., Fromenty, B., 2023. Acetaminophen-induced hepatotoxicity in obesity and nonalcoholic fatty liver disease: a critical review. Livers 3, 33–53. https://doi.org/10.3390/livers3010003.

Bell, C.C., Lauschke, V.M., Vorrink, S.U., Palmgren, H., Duffin, R., Andersson, T.B., Ingelman-Sundberg, M., 2017. Transcriptional, functional, and mechanistic comparisons of stem cell-derived hepatocytes, HepaRG cells, and three-dimensional human hepatocyte spheroids as predictive in vitro systems for drug-induced liver injury. Drug Metab. Dispos. 45, 419–429. https://doi.org/10.1124/dmd.116.074369.

Boeckmans, J., Natale, A., Rombaut, M., Buyl, K., Cami, B., De Boe, V., Heymans, A., Rogiers, V., De Kock, J., Vanhaecke, T., Rodrigues, R.M., 2020. Human hepatic in vitro models reveal distinct anti-NASH potencies of PPAR agonists. Cell Biol. Toxicol. https://doi.org/10.1007/s10565-020-09544-2.

Bucher, S., Jalili, P., Le Guillou, D., Begriche, K., Rondel, K., Martinais, S., Zalko, D., Corlu, A., Robin, M.-A., Fromenty, B., 2017. Bisphenol A induces steatosis in HepaRG cells using a model of perinatal exposure. Environ. Toxicol. 32, 1024–1036. https://doi.org/10.1002/tox.22301.

Bucher, S., Tête, A., Podechard, N., Liamin, M., Le Guillou, D., Chevanne, M., Coulouarn, C., Imran, M., Gallais, I., Fernier, M., Hamdaoui, Q., Robin, M.-A., Sergent, O., Fromenty, B., Lagadic-Gossmann, D., 2018. Co-exposure to benzo[a] pyrene and ethanol induces a pathological progression of liver steatosis in vitro and in vivo. Sci. Rep. 8 https://doi.org/10.1038/s41598-018-24403-1.

Cerec, V., Glaise, D., Garnier, D., Morosan, S., Turlin, B., Drenou, B., Gripon, P., Kremsdorf, D., Guguen-Guillouzo, C., Corlu, A., 2007. Transdifferentiation of hepatocyte-like cells from the human hepatoma HepaRG cell line through bipotent progenitor. Hepatology 45, 957–967. https://doi.org/10.1002/hep.21536.

Chanput, W., Mes, J.J., Wichers, H.J., 2014. THP-1 cell line: an in vitro cell model for immune modulation approach. Int. Immunopharmacol. 23, 37–45. https://doi.org/10.1016/j.intimp.2014.08.002.

Chomchai, S., Chomchai, C., 2018. Being overweight or obese as a risk factor for acute liver injury secondary to acute acetaminophen overdose. Pharmacoepidemiol. Drug Saf. 27, 19–24. https://doi.org/10.1002/pds.4339.

Conaghan, P.G., Arden, N., Avouac, B., Migliore, A., Rizzoli, R., 2019. Safety of paracetamol in osteoarthritis: what does the literature say? Drugs Aging 36, 7–14. https://doi.org/10.1007/s40266-019-00658-9.

Dornas, W., Glaise, D., Bodin, A., Sharanek, A., Burban, A., Le Guillou, D., Robert, S., Dutertre, S., Aninat, C., Corlu, A., Lagente, V., 2019. Endotoxin regulates matrix genes increasing reactive oxygen species generation by intercellular communication between palmitate-treated hepatocyte and stellate cell. J. Cell. Physiol. 234, 122–133. https://doi.org/10.1002/jcp.27175.

EFSA Scientific Committee, Hardy, A., Benford, D., Halldorsson, T., Jeger, M.J., Knutsen, K.H., More, S., Mortensen, A., Naegeli, H., Noteborn, H., Ockleford, C., Ricci, A., Rychen, G., Silano, V., Solecki, R., Turck, D., Aerts, M., Bodin, L., Davis, A., Edler, L., Gundert-Remy, U., Sand, S., Slob, W., Bottex, B., Abrahantes, J.C., Marques, D.C., Kass, G., Schlatter, J.R., 2017. Update: use of the benchmark dose approach in risk assessment. EFS2 15. https://doi.org/10.2903/j.efsa.2017.4658.

FDA, 1996. Depacon (Valproate Sodium), for Intravenous Injection. https://s3-us-west-2.amazonaws.com/drugbank/fda_labels/DB00313.pdf?1556726690.

FDA, 1999. Rezulin® (Troglitazone) Tablets. https://www.accessdata.fda.gov/drugsatfda_docs/label/1999/20720s12lbl.pdf.

Ferron, P.-J., Le Daré, B., Steichen, C., Babina, E., Pelletier, R., Hauet, T., Morel, I., Tarte, K., Reizine, F., Clément, B., Fromenty, B., Gicquel, T., 2021. Molecular networking for drug toxicity studies: the case of hydroxychloroquine in COVID-19 patients. Int. J. Mol. Sci. 23, 82. https://doi.org/10.3390/ijms23010082.

Fraslin, J.m., Kneip, B., Vaulont, S., Glaise, D., Munnich, A., Guguen-Guillouzo, C., 1985. Dependence of hepatocyte-specific gene expression on cell-cell interactions in primary culture. EMBO J. 4, 2487–2491. https://doi.org/10.1002/j.1460-2075.1985.tb03960.x.

French public data base of drugs, 2022. Résumé des caractéristiques du produit - PARACETAMOL CARELIDE 10 mg/ml, solution pour perfusion - Base de données publique des médicaments [WWW Document]. URL. https://base-donnees-publique.medicaments.gouv.fr/affichageDoc.php?specid=66534880&typedoc=R (accessed 12.15.22).

Fromenty, B., 2013. Drug-induced liver injury in obesity. J. Hepatol. 58, 824–826. https://doi.org/10.1016/j.jhep.2012.12.018.

Gicquel, T., Robert, S., Loyer, P., Victoni, T., Bodin, A., Ribault, C., Gleonnec, F., Couillin, I., Boichot, E., Lagente, V., 2015. IL-1β production is dependent on the activation of purinergic receptors and NLRP3 pathway in human macrophages. FASEB J. 29, 4162–4173. https://doi.org/10.1096/fj.14-267393.

Guillocheau, E., Garcia, C., Drouin, G., Richard, L., Catheline, D., Legrand, P., Rioux, V., 2019. Retroconversion of dietary trans-vaccenic (trans-C18:1 n-7) acid to trans-palmitoleic acid (trans-C16:1 n-7): proof of concept and quantification in both cultured rat hepatocytes and pregnant rats. J. Nutr. Biochem. 63, 19–26. https://doi.org/10.1016/j.jnutbio.2018.09.010.

Gunness, P., Mueller, D., Shevchenko, V., Heinzle, E., Ingelman-Sundberg, M., Noor, F., 2013. 3D organotypic cultures of human HepaRG cells: a tool for in vitro toxicity studies. Toxicol. Sci. 133, 67–78. https://doi.org/10.1093/toxsci/kft021.

Ikeda, T., 2011. Drug-induced idiosyncratic hepatotoxicity: prevention strategy developed after the troglitazone case. Drug Metab. Pharmacokinet. 26, 60–70. https://doi.org/10.2133/dmpk.DMPK-10-RV-090.

Khadka, K.K., Chen, M., Liu, Z., Tong, W., Wang, D., 2020. Integrating adverse outcome pathways (AOPs) and high throughput in vitro assays for better risk evaluations, a study with drug-induced liver injury (DILI). ALTEX 37, 187–196. https://doi.org/10.14573/altex.1908151.

Kuiper, H.C., Wei, N., McGunigale, S.L., Vesper, H.W., 2018. Quantitation of trans-fatty acids in human blood via isotope dilution-gas chromatography-negative chemical ionization-mass spectrometry. J. Chromatogr. B Analyt. Technol. Biomed. Life Sci. 1076, 35–43. https://doi.org/10.1016/j.jchromb.2017.12.038.

Lazarus, H.M., Blumer, J.L., Yanovich, S., Schlamm, H., Romero, A., 2002. Safety and pharmacokinetics of oral voriconazole in patients at risk of fungal infection: a dose escalation study. J. Clin. Pharmacol. 42, 395–402.

Le Guillou, D., Bucher, S., Begriche, K., Hoët, D., Lombès, A., Labbe, G., Fromenty, B., 2018. Drug-induced alterations of mitochondrial DNA homeostasis in steatotic and nonsteatotic HepaRG cells. J. Pharmacol. Exp. Ther. 365, 711–726. https://doi.org/10.1124/jpet.117.246751.

Leite, S.B., Roosens, T., El Taghdouini, A., Mannaerts, I., Smout, A.J., Najimi, M., Sokal, E., Noor, F., Chesne, C., van Grunsven, L.A., 2016. Novel human hepatic organoid model enables testing of drug-induced liver fibrosis in vitro. Biomaterials 78, 1–10. https://doi.org/10.1016/j.biomaterials.2015.11.026.

Lemarié, F., Cavalier, J.-F., Garcia, C., Boissel, F., Point, V., Catheline, D., Legrand, P., Carrière, F., Rioux, V., 2016. Effect of preduodenal lipase inhibition in suckling rats on dietary octanoic acid (C8:0) gastric absorption and plasma octanoylated ghrelin concentration. Biochim. Biophys. Acta 1861, 1111–1120. https://doi.org/10.1016/j.bbalip.2016.06.009.

Massart, J., Fromenty, B., 2017. Role of nonalcoholic fatty liver disease as risk factor for drug-induced hepatotoxicity. J. Clin. Translat. Res. https://doi.org/10.18053/jctres.03.2017S1.006.

Massart, J., Begriche, K., Moreau, C., Fromenty, B., 2017. Role of nonalcoholic fatty liver disease as risk factor for drug-induced hepatotoxicity. J. Clin. Translat. Res. 3, 212–232. https://doi.org/10.18053/jctres.03.2017S1.006.

Massart, J., Begriche, K., Corlu, A., Fromenty, B., 2022. Xenobiotic-induced aggravation of metabolic-associated fatty liver disease. IJMS 23, 1062. https://doi.org/10.3390/ijms23031062.

Messner, C.J., Mauch, L., Suter-Dick, L., 2019. Bile salts regulate CYP7A1 expression and elicit a fibrotic response and abnormal lipid production in 3D liver microtissues. Toxicol. In Vitro 60, 261–271. https://doi.org/10.1016/j.tiv.2019.06.002.

Michaut, A., Moreau, C., Robin, M.-A., Fromenty, B., 2014. Acetaminophen-induced liver injury in obesity and nonalcoholic fatty liver disease. Liver Int. 34, e171–e179. https://doi.org/10.1111/liv.12514.

Michaut, A., Le Guillou, D., Moreau, C., Bucher, S., McGill, M.R., Martinais, S., Gicquel, T., Morel, I., Robin, M.-A., Jaeschke, H., Fromenty, B., 2016. A cellular model to study drug-induced liver injury in nonalcoholic fatty liver disease: application to acetaminophen. Toxicol. Appl. Pharmacol. 292, 40–55. https://doi.org/10.1016/j.taap.2015.12.020.

Müller, F.A., Sturla, S.J., 2019. Human in vitro models of nonalcoholic fatty liver disease. In: Current Opinion in Toxicology, Systems Toxicology, 16, pp. 9–16. https://doi.org/10.1016/j.cotox.2019.03.001.

Nascimbeni, F., Pellegrini, E., Lugari, S., Mondelli, A., Bursi, S., Onfiani, G., Carubbi, F., Lonardo, A., 2019. Statins and nonalcoholic fatty liver disease in the era of precision medicine: more friends than foes. Atherosclerosis 284, 66–74. https://doi.org/10.1016/j.atherosclerosis.2019.02.028.

Perumpail, B.J., Khan, M.A., Yoo, E.R., Cholankeril, G., Kim, D., Ahmed, A., 2017. Clinical epidemiology and disease burden of nonalcoholic fatty liver disease. World J. Gastroenterol. 23, 8263–8276. https://doi.org/10.3748/wjg.v23.i47.8263.

Porceddu, M., Buron, N., Roussel, C., Labbe, G., Fromenty, B., Borgne-Sanchez, A., 2012. Prediction of liver injury induced by chemicals in human with a multiparametric assay on isolated mouse liver mitochondria. Toxicol. Sci. 129, 332–345. https://doi.org/10.1093/toxsci/kfs197.

Rinella, M.E., Lazarus, J.V., Ratziu, V., Francque, S.M., Sanyal, A.J., Kanwal, F., Romero, D., Abdelmalek, M.F., Anstee, Q.M., Arab, J.P., Arrese, M., Bataller, R., Beuers, U., Boursier, J., Bugianesi, E., Byrne, C.D., Castro Narro, G.E., Chowdhury, A., Cortez-Pinto, H., Cryer, D.R., Cusi, K., El-Kassas, M., Klein, S., Eskridge, W., Fan, J., Gawrieh, S., Guy, C.D., Harrison, S.A., Kim, S.U., Koot, B.G., Korenjak, M., Kowdley, K.V., Lacaille, F., Loomba, R., Mitchell-Thain, R., Morgan, T. R., Powell, E.E., Roden, M., Romero-Gómez, M., Silva, M., Singh, S.P., Sookoian, S. C., Spearman, C.W., Tiniakos, D., Valenti, L., Vos, M.B., Wong, V.W.-S., Xanthakos, S., Yilmaz, Y., Younossi, Z., Hobbs, A., Villota-Rivas, M., Newsome, P.N., on behalf of the NAFLD Nomenclature consensus group, 2023. A multisociety Delphi consensus statement on new fatty liver disease nomenclature. Hepatology. https://doi.org/10.1097/HEP.0000000000000520.

Rose, S., Cuvellier, M., Ezan, F., Carteret, J., Bruyère, A., Legagneux, V., Nesslany, F., Baffet, G., Langouët, S., 2021. DMSO-free highly differentiated HepaRG spheroids for chronic toxicity, liver functions and genotoxicity studies. Arch. Toxicol. https://doi.org/10.1007/s00204-021-03178-x.

Ruoß, M., Vosough, M., Königsrainer, A., Nadalin, S., Wagner, S., Sajadian, S., Huber, D., Heydari, Z., Ehnert, S., Hengstler, J.G., Nussler, A.K., 2020. Towards improved hepatocyte cultures: progress and limitations. Food Chem. Toxicol. 138, 111188 https://doi.org/10.1016/j.fct.2020.111188.

Schinagl, M., Tomin, T., Gindlhuber, J., Honeder, S., Pfleger, R., Schittmayer, M., Trauner, M., Birner-Gruenberger, R., 2021. Proteomic changes of activated hepatic stellate cells. Int. J. Mol. Sci. 22, 12782. https://doi.org/10.3390/ijms222312782.

Schmidt, U., Weigert, M., Broaddus, C., Myers, G., 2018. Cell detection with star-convex polygons. In: Frangi, A.F., Schnabel, J.A., Davatzikos, C., Alberola-López, C., Fichtinger, G. (Eds.), Medical Image Computing and Computer Assisted Intervention – MICCAI 2018, Lecture Notes in Computer Science. Springer International Publishing, Cham, pp. 265–273. https://doi.org/10.1007/978-3-030-00934-2_30.

Sullivan, K.E., Kumar, S., Liu, X., Zhang, Y., De Koning, E., Li, Y., Yuan, J., Fan, F., 2022. Uncovering the roles of dihydropyrimidine dehydrogenase in fatty-acid induced steatosis using human cellular models. Sci. Rep. 12, 14109. https://doi.org/10.1038/s41598-022-17860-2.

Tarantino, G., Conca, P., Basile, V., Gentile, A., Capone, D., Polichetti, G., Leo, E., 2007. A prospective study of acute drug-induced liver injury in patients suffering from non-alcoholic fatty liver disease. Hepatol. Res. 37, 410–415. https://doi.org/10.1111/j.1872-034X.2007.00072.x.

Teng, Y., Zhao, Z., Tasnim, F., Huang, X., Yu, H., 2021. A scalable and sensitive steatosis chip with long-term perfusion of in situ differentiated HepaRG organoids. Biomaterials 275, 120904. https://doi.org/10.1016/j.biomaterials.2021.120904.

van Kuilenburg, A.B.P., 2004. Dihydropyrimidine dehydrogenase and the efficacy and toxicity of 5-fluorouracil. Eur. J. Cancer 40, 939–950. https://doi.org/10.1016/j.ejca.2003.12.004.

van Os, E.A., Cools, L., Eysackers, N., Szafranska, K., Smout, A., Verhulst, S., Reynaert, H., McCourt, P., Mannaerts, I., van Grunsven, L.A., 2022. Modelling fatty liver disease with mouse liver-derived multicellular spheroids. Biomaterials 290, 121817. https://doi.org/10.1016/j.biomaterials.2022.121817.

Vieira Silva, A., Ringblom, J., Moldeus, P., Törnqvist, E., Öberg, M., 2021. Benchmark dose-response analyses for multiple endpoints in drug safety evaluation. Toxicol. Appl. Pharmacol. 433, 115732 https://doi.org/10.1016/j.taap.2021.115732.

Wang, Y., Wang, H., Deng, P., Tao, T., Liu, H., Wu, S., Chen, W., Qin, J., 2020. Modeling human nonalcoholic fatty liver disease (NAFLD) with an organoids-on-a-chip system. ACS Biomater Sci. Eng. 6, 5734–5743. https://doi.org/10.1021/acsbiomaterials.0c00682.

Wy, K., B, N, K, H, 2007. Alternative pharmacokinetics of S-1 components, 5-fluorouracil, dihydrofluorouracil and alpha-fluoro-beta-alanine after oral administration of S-1 following total gastrectomy. Cancer Sci. 98 https://doi.org/10.1111/j.1349-7006.2007.00573.x.

Xu, L., Hui, A.Y., Albanis, E., Arthur, M.J., O'Byrne, S.M., Blaner, W.S., Mukherjee, P., Friedman, S.L., Eng, F.J., 2005. Human hepatic stellate cell lines, LX-1 and LX-2: new tools for analysis of hepatic fibrosis. Gut 54, 142–151. https://doi.org/10.1136/gut.2004.042127.

Yaegashi, A., Yoshida, K., Suzuki, N., Shimada, I., Tani, Y., Saijo, Y., Toyama, A., 2020. A case of severe hepatotoxicity induced by cisplatin and 5-fluorouracil. Int. Canc. Conf. J. 9, 24–27. https://doi.org/10.1007/s13691-019-00394-2.

Yan, L., Messner, C.J., Zhang, X., Suter-Dick, L., 2021. Assessment of fibrotic pathways induced by environmental chemicals using 3D-human liver microtissue model. Environ. Res. 194, 110679 https://doi.org/10.1016/j.envres.2020.110679.

Zahmatkesh, E., Othman, A., Braun, B., Aspera, R., Ruoß, M., Piryaei, A., Vosough, M., Nüssler, A., 2022. In vitro modeling of liver fibrosis in 3D microtissues using scalable micropatterning system. Arch. Toxicol. https://doi.org/10.1007/s00204-022-03265-7.